Immune cell infiltration and cytokine secretion analysis reveal a non-inflammatory microenvironment of medulloblastoma

SHUO DIAO*, CHUNYU GU*, HONGWEI ZHANG and CHUNJIANG YU

Department of Neurosurgery, Sanbo Brain Hospital, Capital Medical University, Beijing 100093, P.R. China

Received June 30, 2020; Accepted September 29, 2020

DOI: 10.3892/ol.2020.12260

Abstract. Medulloblastoma (MB) is the most common lethal malignant pediatric brain tumor. Adjuvant immunotherapy for medulloblastoma has been proposed in both pre-clinical and clinical practice. To provide a precision strategy of designing immunotherapy for MB, the present study performed a descriptive analysis of immune microenvironment in a cohort and compared the differences between four subgroups of MB. Subtypes (WNT, SHH Group 3 and Group 4) of medulloblastoma were identified using K-means clustering according to the expression of signature genes. Tumor infiltrating immune cell population was assessed by both bio-informative algorithm based on gene expression and immunohistochemistry staining. Cytokines in tumor microenvironment were detected using Luminex. Gene Set Enrichment Analysis demonstrated a raised immune response in the SHH subgroup. Lymphocyte infiltration was low in all four subgroups, while more $CD4^+$ T cells were observed in the Group 4 subtype. Programmed cell death protein 1 (PD1)/ ligand 1 (PD-L1) expression was absent in the cohort. The SHH subtype recruited more activated tumor associated macrophage/microglia compared with the other subgroups. Cytokines within the MB microenvironment were low compared with the glioblastoma samples. In contrast to glioblastoma, the immune microenvironment of pediatric MB is non-inflammatory and does not recruit many immune cells. These observations provide important considerations for the design of immunotherapeutic approaches for MB, such as inducing more lymphocytes into the tumor microenvironment.

Introduction

Pediatric brain tumor is one of the leading causes of cancer-associated mortality in children (1). The incidence rate of childhood and adolescent brain tumors in the United States is approximately 5.67 per 100,000 person-years (2). Medulloblastoma (MB) is the most common malignant pediatric brain tumor, but can also rarely occur in adults. MB is classified into 4 subgroups based on molecular characteristics, as follows: WNT, SHH, Group 3 (G3) and Group 4 (G4) (3). WNT-MBs frequently contain a CTNNB1 mutation, while the SHH subtype contains mutations that activate the SHH pathway (3). The Group 3 subtype is characterized by overexpression of MYC, while Group 4 is the only subgroup lacking upregulated MYC expression (4). Currently, the standard of care is maximal surgical resection followed by risk adapted cranio-spinal irradiation (CSI) and adjuvant chemotherapy, and the 5-year overall survival rates for patients with average- and high-risk MBs range from 65-85% (5). However, the adverse effects of CSI, including permanent neurocognitive disability, growth disturbances, infertility and hearing loss, continue to affect the improving prognosis of MB (6). Thus, it remains critical to identify alternative therapies to delay or omit CSI in children.

Immunotherapy is effective for patients with melanoma, leukemia and other solid tumors (7-10). The importance of lymphocytes and tumor-associated macrophages (TAMs) in the tumor microenvironment has been assessed and is considered a key factor of immunotherapy response (11,12). However, little is known about the comprehensive immune infiltration in brain tumor, particularly in MB. Due to limited patient sample sizes and preclinical models, the status and function of immune microenvironment remains controversial. Vermeulen *et al* (13) reported no programmed cell death protein ligand 1 (PD-L1) expression in 26 MB cohorts, suggesting limited or no added value for immunotherapy with PD1/PD-L1 blockers in MB. Conversely, Martin *et al* (14) demonstrated that PD-L1 is expressed at low levels in MB to facilitate immune escape.

A comprehensive heterogeneity within four subgroups is one of the most actively studied fields in MB (15). However, the characterization of the immune microenvironment in the four subgroups remains unclear. Bockmayr *et al* (16) assessed the subgroup-specific immune microenvironment in MB using an open gene expression database. However, data only based on gene expression provides limited reliability and may fail to provide information on the functional status. For example, cytokines and chemokines play an important role in modulating the MB immune microenvironment and tumor progression (17,18). Thus, the present study compared

Correspondence to: Dr Chunjiang Yu, Department of Neurosurgery, Sanbo Brain Hospital, Capital Medical University, 50 Yikesong Road, Beijing 10093, P.R. China
E-mail: cjyu1955@sina.com

*Contributed equally

Key words: medulloblastoma, tumor-associated macrophage, tumor-infiltrating lymphocyte, cytokine, immune microenvironment

69 cytokines/chemokines within the four MB subgroups and glioblastoma multiform (GBM). Taken together, the results of the present study provide a novel comprehensive description of the immune microenvironment of MB, which may help guide clinical translation of immune-related therapies.

Materials and methods

Human tissue samples. The present study was approved by the Ethics Committee of Sanbo Brain Hospital, Capital Medical University (Beijing, China; approval no. SBNK-YJ-2018-013-01). and all procedures were performed in accordance with the 1964 Declaration of Helsinki (19). All patients or their guardians provided written informed consent prior to the study start. A total of 19 MB tissues, three GBM tissues and two peritumoral normal brain tissue samples were collected from patients who underwent surgical resection at Sanbo Brain Hospital, Capital Medical University between January 2017 and December 2018. Snap-frozen tissues were labeled and stored at -80˚C until subsequent experimentation. Patients characteristics, including sex, age and collection date are listed in Table I.

RNA sequencing. Total RNA was extracted from snap-frozen tissues using TRIzol® reagent (Invitrogen; Thermo Fisher Scientific, Inc.). RNA quality was assessed using the Bioanalyzer 2200 (Agilent Technologies, Inc.) and RNA integrity number >6.0 was qualified for cDNA library construction. The cDNA libraries were constructed for each pooled RNA sample using the NEBNext UltraTM Directional RNA Library Prep kit (cat. no. E7420S; New England BioLabs, Inc.) for Illumina, according to the manufacturer's instructions. The following steps were performed: mRNA was fragmented into 150-200 bp using divalent cations at 94˚C for 8 min, the cleaved RNA fragments were reverse transcribed into first- and second-strand cDNA, respectively, fragments were end repaired, and A-tailed and ligated with indexed adapters. Target bands were harvested using AMPure XP Beads (Beckman Coulter, Inc.). The products were purified and enriched via PCR to create the final cDNA libraries, and quantified using Agilent2200 software (version A.02.01; Agilent Technologies, Inc.). The tagged cDNA libraries were pooled in an equal ratio and used for 150 bp paired-end sequencing in a single lane of the Illumina Nova Seq (https://www.illumina.com/systems/sequencing-platforms/novaseq.html).

K-means clustering. To identify the MB subgroups in the 19 patients with MB, previously reported subgroup-specific signature genes were used for K-means clustering (4). The cluster number was set to four because MB was reported to comprise four distinct molecular variants (4). Each cluster was then analyzed by hierarchical clustering algorithms with squared Pearson correlation as similarity measurement (20).

Gene Set Enrichment Analysis (GSEA). Due to the limited sample size of WNT MB (n=1), GSEA analysis was only preformed in SHH, Group 3 and Group 4. GSEA (version 4.0.3; Broad Institute; www.broadinstitute.org) was used according to the manufacturer's instructions. Briefly, gene expression data matrix was classified into three subgroups (SHH, Group 3 and Group 4). H: hallmark gene sets were downloaded from the MSigDB database (http://software.broadinstitute.org/gsea/msigdb), and the number of permutations was set to 1,000. Gene set enrichment was considered significant at false discovery rate <0.25.

Immunohistochemistry (IHC). Lymphocyte infiltration and PD-L1 expression were assessed via IHC analysis on 4 μm formalin-fixed and paraffin-embedded (FFPE) tissues. Human glioblastoma tissue was used as the positive control for PD-L1 staining. Tissue slides were deparaffinized in xylene for 20 min at room temperature and rehydrated in a descending ethanol series (90-50%). For antigen retrieving, the tissue slides were incubated in EDTA buffer (pH 9.0) (cat. no. E673003; Sangon Biotech, Co., Ltd.) for 8 min at room temperature. Tissue sections were washed three times with phosphate-buffered saline, prior to incubation with 3% H_2O_2 for 10 min at room temperature to inhibit endogenous peroxidase activity. The sections were subsequently blocked with 5% normal goat serum (cat. no. E510009; Sangon Biotech, Co., Ltd.) for 30 min at room temperature and incubated with primary antibodies against CD3 (cat. no. ab16669, 1:100; Abcam) and PD-L1 (cat. no. ab213524, 1:100; Abcam) overnight at 4˚C. The Dako REAL EnVision Detection System (Dako; Agilent Technologies, Inc.) was used as a secondary antibody, according to the manufacturer's protocol. Tissue sections were subsequently dehydrated in an ascending ethanol series (50-90%), cleared with xylene and covered with a coverslip. The sections were observed under a Nikon Eclipse light microscope (magnifications, x20 and x40). The IHC score for CD3 staining was calculated based on the CD3 positive cells/field.

Immunofluorescence (IF). Microglia/macrophage recruitment was assessed via IF analysis on FFPE tissues. Tissue slides were deparaffinized, rehydrated following antigen retrieving and blocked as described for IHC. The sections were incubated with rabbit anti-IBA1 (1:1,000; Wako Pure Chemical Industries, Ltd.) overnight at 4˚C. Subsequently, tissue sections were incubated with AlexaFluor 488 conjugated secondary antibodies (cat. no. R37116, 1:500, Invitrogen; Thermo Fisher Scientific, Inc.) at room temperature for 4 h to detect the primary labeling. Tissue sections were mounted using ProLong Diamond Antifade Mountant with DAPI (cat. no. P36962; Thermo Fisher Scientific, Inc.), and the mounted samples were observed under a confocal microscope (LSM 700; Carl Zeiss AG; magnifications, x40 and x60). Z-stack images were acquired and stacked via maximum intensity project using ImageJ software (version 1.0; National Institutes of Health). IBA-1 positive cells were manually counted and quantified using SPSS 17.0 software (SPSS, Inc.).

Estimating immune signatures. Immune signatures of mRNA markers from 10 cell populations were used to estimate the microenvironment cell populations (MCP), including T cells, $CD8^+$ T cells, cytotoxic T lymphocytes (CTL), B cells, NK cells, monocytic lineage cells, myeloid dendritic cells, neutrophils, fibroblasts and endothelial cells in MB tissues. Microenvironment Cell Population Counter (MCP-Counter) (15) scores were defined as the log2 average expression of the transcriptomic markers for each population.

Table I. Clinicopathological characteristics.

Characteristics	Sex		Age range, (years)	Collection date
	Male, n	Female, n		
MB subtype				
WNT	0	1	8	March 2017
SHH	4	1	3-11	January 2017-December 2018
G3	3	2	8-24	January 2017-March 2018
G4	6	2	7-18	February 2017-December 2018
GBM	1	2	37-58	October 2018-December 2018
Normal	1	1	17-31	May 2018-August 2018

MB, medulloblastoma; GBM, glioblastoma multiform; G3, Group 3; G4, Group 4.

Luminex assay. MB samples were collected during surgery, snap-frozen in liquid nitrogen and stored at -80˚C. The Bio-plex Pro Human Cytokine kit (cat. no. 12007283; Bio-Rad Laboratories, Inc.) and the Bio-Plex Pro Human Chemokine Panel 40-plex kit (cat. no. 171AK99MR2; Bio-Rad Laboratories, Inc.) were used according to the manufacturer's recommendations. Briefly, beads were added to a 96-well plate and washed with Assay Buffer for 30 sec. Samples were added to the plate containing the mixed antibody-linked beads and incubated at room temperature for 1 h, at 850 rpm on a plate shaker. Following the primary incubation, the plates were washed three times with Assay Buffer and subsequently incubated with Detection Antibody for 75 min at room temperature, on a plate shaker. The plates were re-washed, followed by addition of streptavidin-PE. Following incubation for 30 min at room temperature, the plates were washed prior to addition of reading buffer. The plates were analyzed on the Luminex 200 platform (Wayen Biotechnologies, Shanghai, Inc.; www.wayenbio.com). Each sample was measured in duplicate.

Statistical analysis. Statistical analyses were performed using GraphPad Prism 7.0 software (GraphPad Software, Inc.) and SPSS 17.0 software (SPSS, Inc.). All experiments were performed in triplicate and data are presented as the mean ± standard error of the mean. One-way analysis of variance followed by Bonferroni's post hoc test was performed to compare differences between multiple groups. Pearson's correlation analysis was performed to determine the association between cytokine/chemokine protein and RNA expression. $P<0.05$ was considered to indicate a statistically significant difference.

Results

Identification of molecular subgroups of MBs using transcriptional profiling data. To identify WNT, SHH, Group 3 and Group 4 MB, RNA sequencing (RNA-Seq) was performed to obtain gene expression of all MB samples (n=19). According to the previously published 84 subgroup-specific signature genes (4), the present study identified 1 WNT, 5 SHH, 5 Group 3 and 8 Group 4 MBs using K-means clustering. The heatmap demonstrated the distinct patterns of expression of subgroup-specific signature genes among the four MB subgroups (Fig. 1A). The degree of separation of the four subgroups was assessed via principal component analysis, with the WNT subtype demonstrating a distanced separation away from the other three groups. While Group 3 and Group 4 were closer to each other, the SHH subtype demonstrated a clear demarcation from the Group 3 and Group 4 subtypes (Fig. 1B).

Immune response is predominantly elevated in the SHH subgroup. To assess and compare gene expression of the different subgroups of MB, GSEA was performed with RNA-Seq data. Due to the limited sample size of WNT MB, analysis was only performed in the SHH, Group 3 and Group 4 subtypes. A total of 50 hallmark gene sets were downloaded from the MSigDB database, with 6 immune-related gene sets significantly enriched in the SHH subgroup compared with Group 3 in the top 20 enrichment score (ES) gene sets, including inflammatory response, interferon γ response, IL6-JAK-STAT3 signaling, TNF-α signaling via NFKB, interferon α response and IL2-STAT5 signaling (Fig. 2A). Similar results were observed following comparison of the SHH and Group 4 subgroups, suggesting that the SHH subgroup MBs are more involved in the immune microenvironment compared with Group 3 and Group 4 MBs (Fig. 2B).

Tissue-infiltrating immune cell population in the MB subgroups. The MCP-Counter method was used to estimate the population abundance of tissue-infiltrating immune cells in the MB subgroups, using the RNA-Seq data. The expression scores were significantly different between the subgroups in cytotoxic lymphocytes (P=0.0002) and neutrophils (P=0.001). In addition, Group 4 tumors had more cytotoxic lymphocytes and neutrophils compared with tumors from the other subgroups (Fig. 2C).

Lymphocyte infiltration in the MB subgroups. To validate the diverse pattern of lymphocyte infiltration in the four MB subgroups, IHC analysis was performed on the tissue samples for CD3. The results demonstrated that overall CD3 staining in the MB tissues from the four subgroups were minimal, which was consistent with previous studies (13,16). Although the

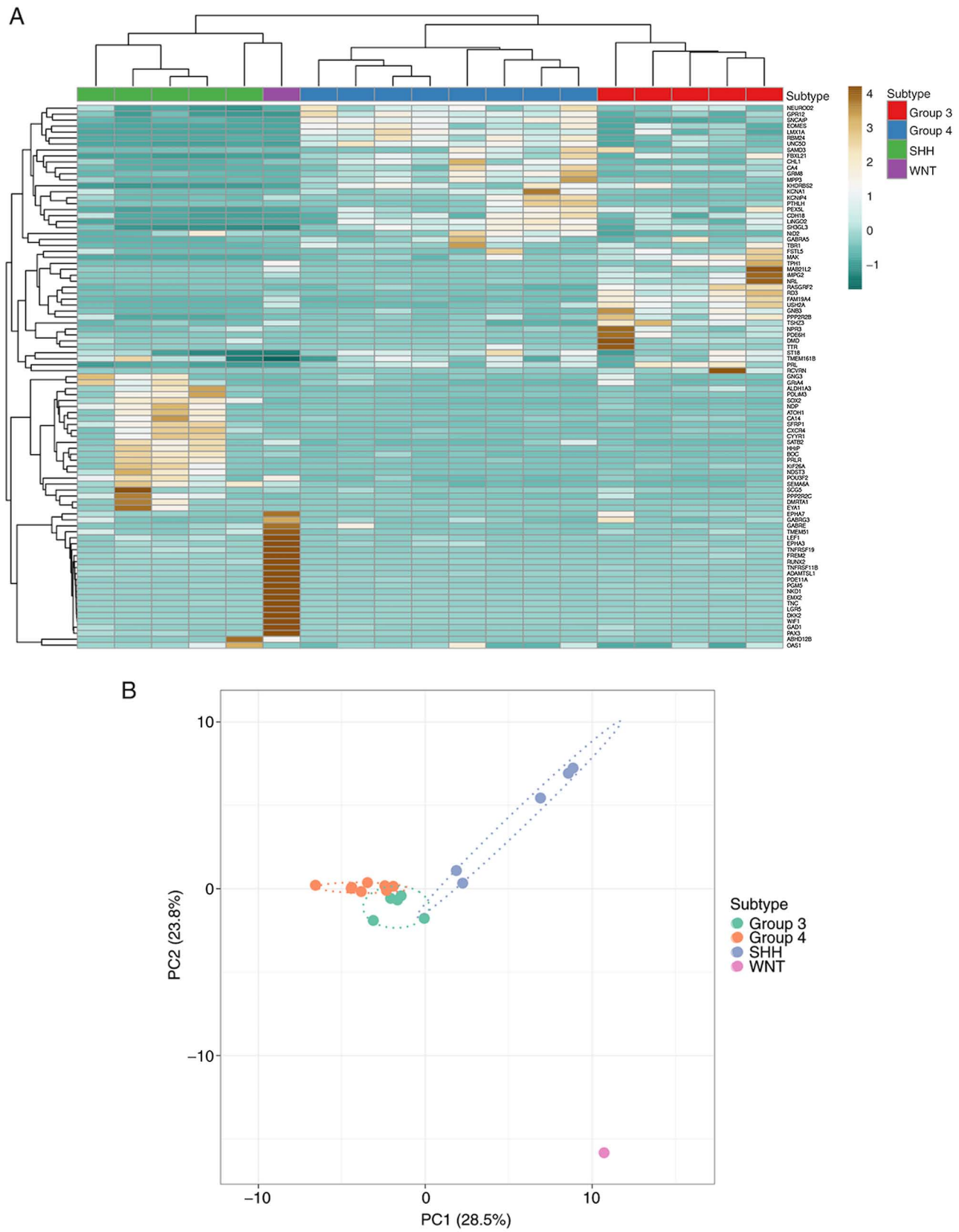

Figure 1. Identification of molecular subgroups. (A) Heatmap of the expression levels of 84 subgroup-specific signature genes. (B) PC analysis demonstrated the degree of separation between the four subgroups. PC, principal component.

number of CD3 positive cells between the subgroups was not significantly different (P=0.0886), tumors from the Group 4 subtype exhibited more CD3 positive lymphocytes infiltration compared with the other subgroups, which was concordant with the MCP-Counter data of the cohort in the present study (Fig. 3A and B). Notably, the majority of CD3 positive cells

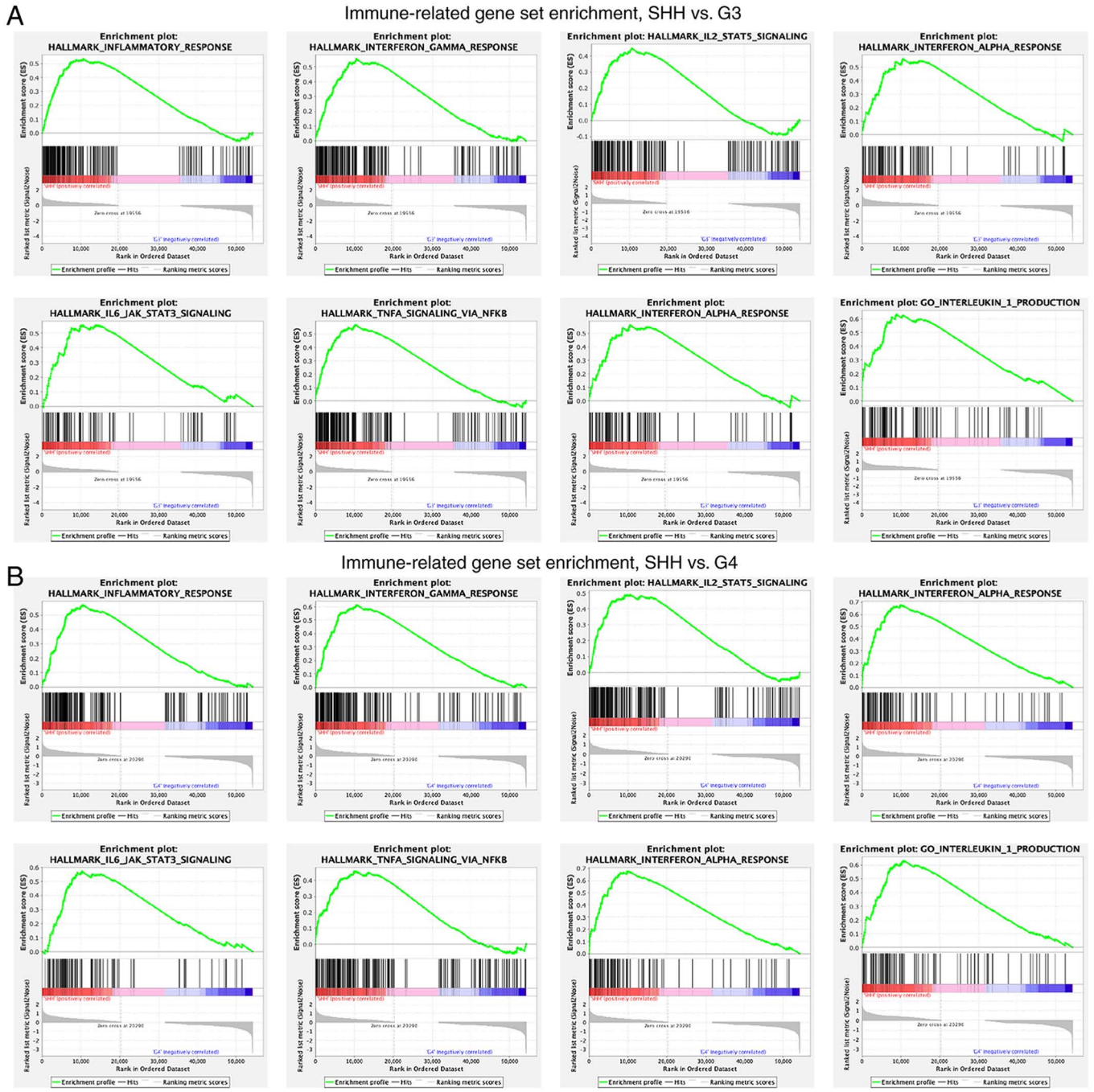

Figure 2. Estimating the immune microenvironment using RNA-seq data. (A) GSEA was performed using the hallmark gene sets downloaded from the MSigDB database on RNA-Seq data, and running enrichment scores for immune-related gene sets were plotted, SHH vs. G3 subtypes. (B) GSEA between the SHH and G4 subtypes. RNA-Seq, RNA sequencing; GSEA, Gene Set Enrichment Analysis;

were localized in the perivascular, suggesting the lack of infiltration of T cells in the tumor mass (Fig. 3A).

The PD1/PD-L1 axis has been investigated and is considered a promising target for immunotherapy in MBs (13,14,21). The present study investigated PD-L1 expression in the patient cohort; however, no positive staining was observed (Fig. 3C). Collectively, these results suggest that lymphocyte infiltration is relatively low in MBs, and the PD1/PD-L1 axis may not be a promising therapeutic target in clinical practice.

Activated macrophage/microglia recruitment in the MB subgroups. Macrophages and microglia have been reported to play vital roles in central nervous system (CNS) inflammation (22). The present study initially identified macrophage/microglia via IF IBA1 staining in both MB tissues and normal cerebellum tissues. While the microglia in normal cerebellum exhibited a resting phenotype with long processes, the MB TAM exhibited an activated phenotype with short or absent processes (Fig. 4A). The morphology of activated TAMs in the four MB subtypes were similar (data not shown), so only the SHH subtype is presented in Fig. 4A. The density of activated TAMs in the MB subgroups was subsequently assessed. The results demonstrated that SHH tumors had more TAMs recruitment compared with tumors in the other subgroups (Fig. 4B and C).

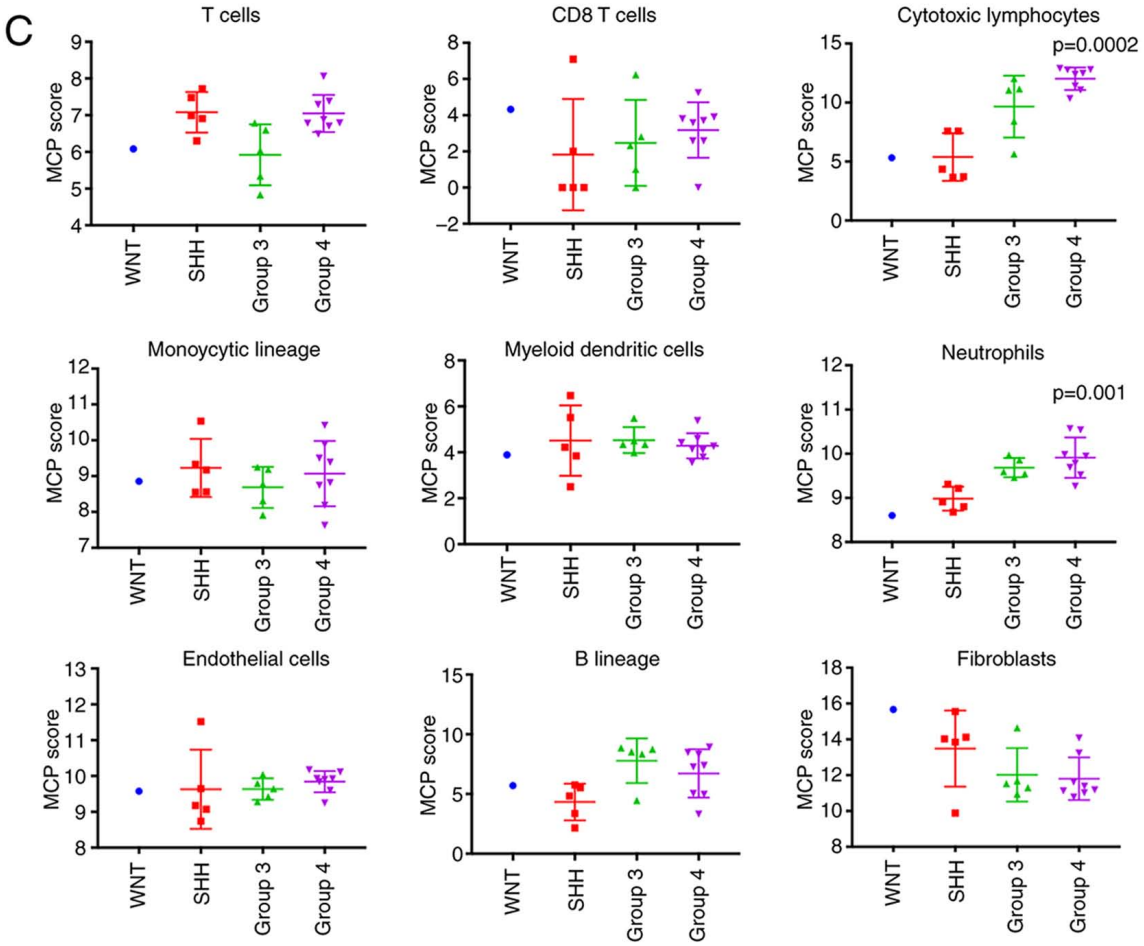

Figure 2. Continued. (C) Estimated expression score of microenvironment cell populations using the MCP counter method. Each plot represents an individual sample, while the bands represent the median and the standard error of the mean. G3, Group 3; G4, Group 4; MCP, microenvironment cell populations.

Cytokine profiling of MB tumors across the four subgroups. Cytokines play a key role in modulating the tumor microenvironment and immune cells infiltration (17). Given that the SHH tumors exhibited more inflammatory compared with the other subgroups, it was speculated that the inflammatory-related cytokines of SHH tumors may differ from the other subgroups. A total of three tumors were collected from the SHH, Group 3 and Group 4 subtypes, respectively, a WNT tumor, three GBM tumors and two normal cerebellum tissues, and multiple cytokine/chemokine was analyzed using Luminex array. K-means hierarchical clustering analysis demonstrated that MB tumors were similar to normal cerebellum, and secreted less cytokines and chemokines compared with GBM tumors (Fig. 5A). These results were consistent with the low expression of cytokine/chemokine-encoding genes. Given the importance of inferring the microenvironment to guide immunotherapy for clinical practice (23), the correlation between the concentration of cytokine/chemokine protein and RNA expression was assessed. Pearson's correlation analysis demonstrated a positive correlation between cytokine/chemokine protein and RNA expression (Fig. 5B). Collectively, these results may explain why MB recruits fewer immune cells to the tumor microenvironment compared with GBM. In addition, the overall expression of cytokine-encoding genes in the RNA-Seq data were low. Most of the Fragments Per Kilobase per Million values were <5, which was considered negative (Fig. 5C).

Discussion

MB is the most common pediatric brain tumor originating from the posterior fossa, and is a leading cause of cancer-associated mortality in children in the United States (1,24). MB is currently classified into four groups based on the molecular pathway characteristics, as follows: WNT, SHH, Group 3 and Group 4 subtypes. In the WNT subtype, the canonical Wnt signaling pathway is upregulated (24). The SHH subtype is defined by activation of the Sonic hedgehog signaling pathway (24). The Group 3 subtype, which has the worst outcome among all MB subtypes, is characterized by amplification of multiple proto-oncogenes, including MYC, PVT1 and SMARCA4 (4). The Group 4 MB subtype is characterized by molecular abnormalities associated with a frequent mutation in the KDM6A gene (25). As suggested in the NCCN guideline (26), patients who have a high risk of relapse should be administrated radiotherapy, which may cause severe cognitive dysfunction (27). Thus, alternative therapeutic strategies are required, among which immunotherapy proves promising (28). Compared with adult brain tumors, less is known about the immune microenvironment

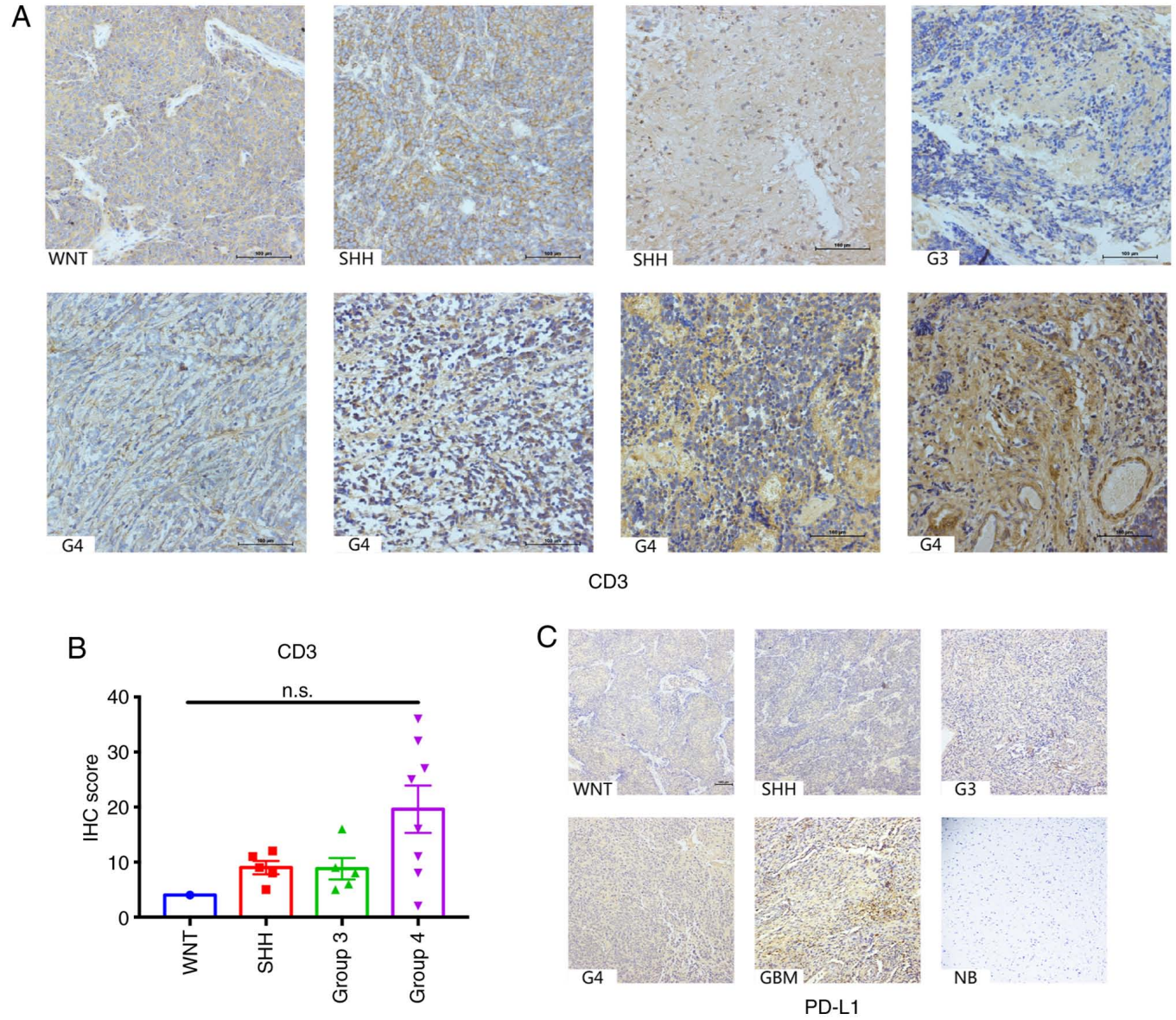

Figure 3. Lymphocyte infiltration and PD-L1 expression in MB. (A) CD3 staining in the four MB subtypes. (B) IHC score for CD3 staining in the four MB subgroups. (C) Negative PD-L1 expression in MB samples. Glioma samples and normal brain tissues were used as the positive and negative controls, respectively. PD-L1, programmed cell death 1 ligand 1; MB, medulloblastoma; NB, normal brain tissue; IHC, immunohistochemistry; n.s., not significant; GBM, glioblastoma multiform; G3, Group 3; G4, Group 4.

of MB due to the limited sample size, which in turn impedes clinical translation attempt for precision immunotherapy. Thus, the present study aimed to investigate the immune microenvironment of the four subtypes of MB in 19 freshly collected MB samples. Bioinformatics and IHC analyses, along with multiple cytokine/chemokine Luminex assay were performed in the hope to provide a comprehensive overview from different dimensions.

In order to compare the distinct immune microenvironment within the four MB subtypes, RNA sequence of the 19 freshly collected MB samples was initially acquired. Based on previously published subtype-related gene signature (4), hierarchical clustering analysis effectively separated the samples into the four subgroups. However, only one WNT MB was identified, which is compatible with a low incidence (~10%) of all MB diagnosis (24). Thus, most of the statistical analyses excluded the WNT subtype due to the limited sample size.

GSEA was performed to compare hallmark pathways in the different subgroups. The results demonstrated that the immune-related gene sets were significantly enriched in the SHH subgroup compared with the G3 and G4 subtypes, suggesting an activated immune phenotype in the SHH subgroup. The immune cell populations were subsequently estimated using the MCP-counter, which uses specific gene signatures to identify eight immune cell populations and two stromal cell populations (29). Among the 10 populations, only cytotoxic lymphocytes and neutrophils exhibited statistical differences. Notably, the G4 subgroup had more immune cell infiltration compared with the SHH subgroup, which exhibited an activated immune phenotype in GSEA. Both analyses were based on transcriptome data; however, the biological implications varied. GESA hallmark gene sets represent specific well-defined biological states, while MCP-Counter estimates the infiltration of immune cell populations (29,30). These bioinformatics

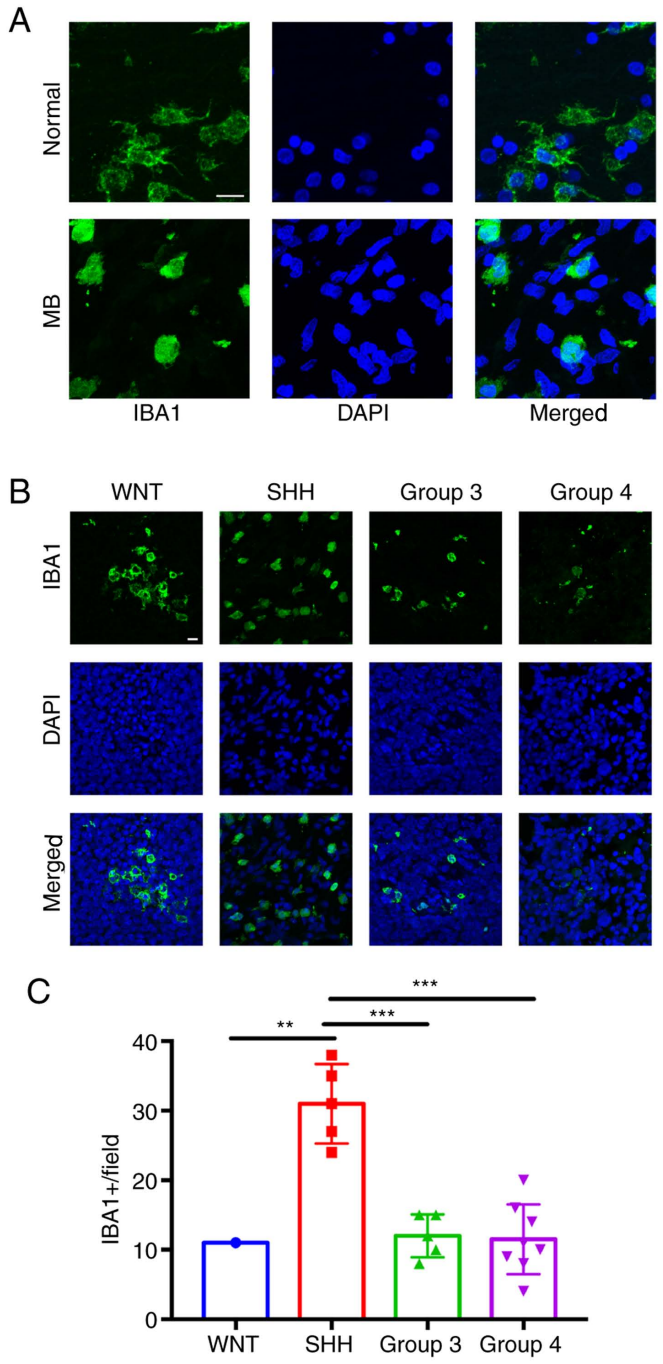

Figure 4. TAMs recruitment in the MB subgroups. (A) IBA1 staining for macrophage/microglia infiltration in the MB microenvironment exhibited an activated phenotype with a shortened process compared with normal brain tissues. Representative images from the SHH subtype. (B) IBA1 expression in the four MB subgroups. (C) Statistical bar for (B). The SHH subtype recruited more TAMs compared with the other subgroups. **P<0.01, ***P<0.001. Scale bar, 50 μm. TAMs, tumor-associated macrophages; MB, medulloblastoma.

data indicated that tumor cells, rather than infiltrated immune cells, activate immune-related pathways in the MB tumor microenvironment. Notably, a similar phenotype was reported in another study on the microenvironment of diffuse intrinsic pontine glioma, which is another non-inflammatory pediatric brain tumor (31).

Given that the G4 subtype exhibited the highest levels of lymphocytes and neutrophil infiltration (Fig. 2C), the present study stained all samples for CD3, PD-L1 and MPO. The results demonstrated that the G4 subtype contained more CD3 positive T cells; however, there were no statistical significant differences compared with the other subgroups. More samples should be involved in the future study to validate if G4 MB have more CD3 positive T cells infiltration than other subgroups.

Previous studies have demonstrated that PD-L1 expression in MB is associated with prognosis and response to immune checkpoint inhibitor (21,32). However, in the present cohort, none of 19 MB samples exhibited positive PD-L1 staining. Consistent with previous findings (13,33), the results of the present study suggest that PD-L1 expression is absent in MB samples. Thus, PD-L1 blockade may not be a feasible strategy for MB therapy. Neutrophils have been reported to promote adult malignant glioma progression, and have been observed in high grade gliomas (34). The present study failed to identify any MPO positive neutrophils in the assessed MB samples however, the MCP-counter score demonstrated positive infiltration. Taken together, these results suggest that neutrophil infiltration is more common in malignant glioma. Prospective studies are required to validate the role of neutrophils in MB.

Microglia are the resident immune cells in the CNS (35). TAMs play an important role in the MB microenvironment, whereby TAM-secreted cytokines, chemokines and growth factors regulate immune function and modulate the interaction of multiple cellular populations within the tumor microenvironment, thus contribute to tumor progression (35). A recent study by Yao *et al* (18) demonstrated that tumor-cell-derived astrocytes produce IL-4 that stimulates microglia to produce IGF1, which in turn induces progression of the SHH subtype in a preclinical mouse model (18). Consistent with previous findings (36,37), the results of the present study suggest that the SHH subtype has a distinct pattern of TAMs infiltration. Thus, it was hypothesized that the SHH subtype secretes distinct cytokines/chemokines. However, the results of the present study demonstrated that the cytokines/chemokines were not associated with this molecular subgroup. The most plausible explanation is that MB secrets none to very low levels of cytokines/chemokines, thus, the difference between subtypes is not significant. To the best of our knowledge, the present study was the first to compare cytokine secretion within MB subtypes and GBM. Although the overall expression of cytokines is very low, exogenous administration of cytokines or inhibitors may be a useful target for immunotherapy. For example, TGF-β neutralization facilitated NK-cell induces MB suppression (38).

Collectively, the results of the present study suggest a 'cold' immune microenvironment of MB, which guides the strategy of MB immunotherapy towards inducing more immune cells into the tumor microenvironment. The capacity of CTL infiltration in MB is another issue due to the blood brain barrier (28). Thus, intratumorally delivering T cells may prove useful. For example, intratumorally delivered anti-human epidermal growth factor receptor 2 CAR-T cells have demonstrated effective preclinical efficacy *in vitro* and in mouse medulloblastoma treatment (39).

Taken together, the results of the present study suggest that the immune microenvironment of pediatric MB is non-

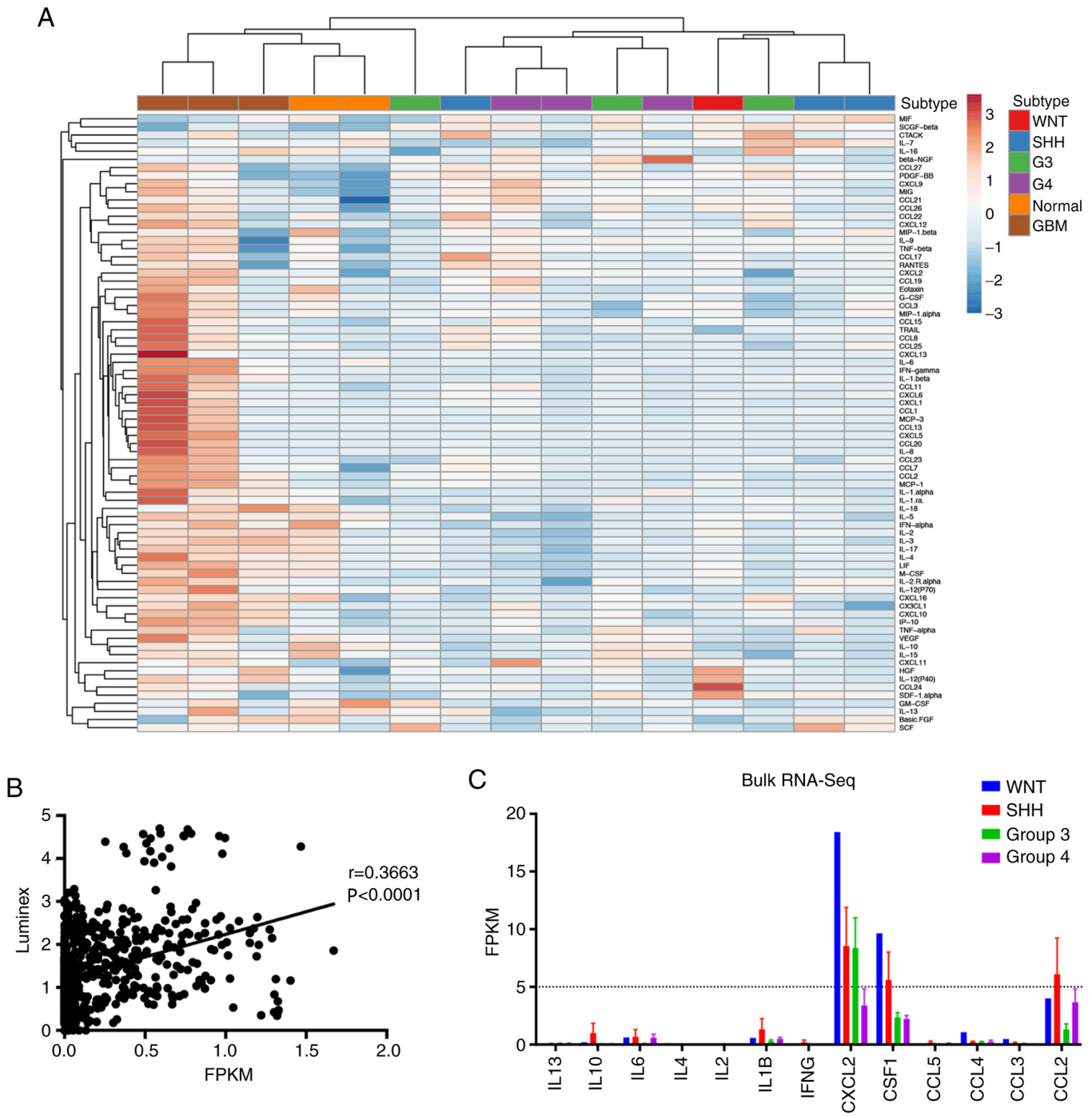

Figure 5. Cytokines and chemokines profile in the MB subgroups. (A) Hierarchical clustering of mean values of cytokines and chemokines in the MB subgroups, normal brain tissues and glioma samples. Each column represents the average score assessed in triplicate, and each row represents a separately measured cytokine or chemokine. (B) Pearson's correlation analysis of cytokine concentration and gene expression. y-axis represents the cytokine concentration measured by Luminex, while the x-axis represents the cytokine-encoding gene expression by RNA-Seq. (C) Bar chart of FPKM of cytokine-encoding genes. Dashed line represents FPKM=5. MB, medulloblastoma; RNA-Seq, RNA sequencing; G3, Group 3; G4, Group 4; GBM, glioblastoma multiform; IL, interleukin; IFNγ, interferon-gamma; CXCL2, C-X-C motif ligand 2; CSF1, colony stimulating factor 1; CCL, C-C motif ligand 2; FPKM, fragments per kilobase per million.

inflammatory and does not recruit as much immune cells compared with glioblastoma. Targeting the PD1/PD-L1 axis for MB treatment may not be a plausible strategy due to the absence of PD-L1 expression. Taken together, the results of the present study provide novel insight into the design of immunotherapeutic approaches for MB, such as CAR-T therapy which may induce more cytotoxic lymphocytes into the tumor microenvironment.

Acknowledgements

Not applicable.

Funding

The present study was funded by the Beijing Postdoctoral Research Foundation (grant no. ZZ2019-02).

Availability of data and materials

The datasets used during the present study are available from the corresponding author upon reasonable request.

Authors' contributions

SD and CG performed the experiments, analyzed the data and drafted the initial manuscript. HZ acquired the patient samples and performed the histology scoring. CY conceived and designed the present study, and supervised the project. All authors have read and approved the final manuscript.

Ethical approval and consent to participate

The present study was approved by the Ethics Committee of Sanbo Brain Hospital Capital Medical University (Beijing, China; approval no. SBNK-YJ-2018-013-01), and all procedures were performed in accordance with the 1964 Declaration of Helsinki (19). All patients or their guardians provided written informed consent prior to the study start.

Patients consent for publication

Not applicable.

Competing interests

The authors declare that they have no competing interests.

References

1. Burstein R, Henry NJ, Collison ML, Marczak LB, Sligar A, Watson S, Marquez N, Abbasalizad-Farhangi M, Abbasi M, Abd-Allah F, *et al*: Mapping 123 million neonatal, infant and child deaths between 2000 and 2017. Nature 574: 353-358, 2019.
2. Ostrom QT, Gittleman H, Xu J, Kromer C, Wolinsky Y, Kruchko C and Barnholtz-Sloan JS: CBTRUS Statistical Report: Primary Brain and Other Central Nervous System Tumors Diagnosed in the United States in 2009-2013. Neuro Oncol 18 (suppl_5): v1-v75, 2016.
3. Millard NE and De Braganca KC: Medulloblastoma. J Child Neurol 31: 1341-1353, 2016.
4. Northcott PA, Korshunov A, Witt H, Hielscher T, Eberhart CG, Mack S, Bouffet E, Clifford SC, Hawkins CE, French P, *et al*: Medulloblastoma comprises four distinct molecular variants. J Clin Oncol 29: 1408-1414, 2011.
5. Sirachainan N, Nuchprayoon I, Thanarattanakorn P, Pakakasama S, Lusawat A, Visudibhan A, Dhanachai M, Larbcharoensub N, Amornfa J, Shotelersuk K, *et al*: Outcome of medulloblastoma in children treated with reduced-dose radiation therapy plus adjuvant chemotherapy. J Clin Neurosci 18: 515-519, 2011.
6. Doger de Speville E, Robert C, Perez-Guevara M, Grigis A, Bolle S, Pinaud C, Dufour C, Beaudré A, Kieffer V, Longaud A, *et al*: Relationships between regional radiation doses and cognitive decline in children treated with cranio-Spinal irradiation for posterior fossa tumors. Front Oncol 7: 166, 2017.
7. Cuevas LM and Daud AI: Immunotherapy for melanoma. Semin Cutan Med Surg 37: 127-131, 2018.
8. Barsan V, Ramakrishna S and Davis KL: Immunotherapy for the treatment of acute lymphoblastic leukemia. Curr Oncol Rep 22: 11, 2020.
9. Naylor EC, Desani JK and Chung PK: Targeted therapy and immunotherapy for lung cancer. Surg Oncol Clin N Am 25: 601-609, 2016.
10. Morrison AH, Byrne KT and Vonderheide RH: Immunotherapy and prevention of pancreatic cancer. Trends Cancer 4: 418-428, 2018.
11. Lorenzo-Sanz L and Muñoz P: Tumor-infiltrating immunosuppressive cells in cancer-cell plasticity, tumor progression and therapy response. Cancer Microenviron 12: 119-132, 2019.
12. Kennedy BC, Showers CR, Anderson DE, Anderson L, Canoll P, Bruce JN and Anderson RC: Tumor-associated macrophages in glioma: Friend or foe? J Oncol 2013: 486912, 2013.
13. Vermeulen JF, Van Hecke W, Adriaansen EJM, Jansen MK, Bouma RG, Villacorta Hidalgo J, Fisch P, Broekhuizen R, Spliet WGM, Kool M, *et al*: Prognostic relevance of tumor-infiltrating lymphocytes and immune checkpoints in pediatric medulloblastoma. OncoImmunology 7: e1398877, 2017.
14. Martin AM, Nirschl CJ, Polanczyk MJ, Bell WR, Nirschl TR, Harris-Bookman S, Phallen J, Hicks J, Martinez D, Ogurtsova A, *et al*: PD-L1 expression in medulloblastoma: An evaluation by subgroup. Oncotarget 9: 19177-19191, 2018.
15. Cavalli FMG, Remke M, Rampasek L, Peacock J, Shih DJH, Luu B, Garzia L, Torchia J, Nor C, Morrissy AS, *et al*: Intertumoral heterogeneity within medulloblastoma subgroups. Cancer Cell 31: 737-754.e6, 2017.
16. Bockmayr M, Mohme M, Klauschen F, Winkler B, Budczies J, Rutkowski S and Schüller U: Subgroup-specific immune and stromal microenvironment in medulloblastoma. Oncoimmunology 7: e1462430, 2018.
17. Gieryng A, Pszczolkowska D, Walentynowicz KA, Rajan WD and Kaminska B: Immune microenvironment of gliomas. Lab Invest 97: 498-518, 2017.
18. Yao M, Ventura PB, Jiang Y, Rodriguez FJ, Wang L, Perry JSA, Yang Y, Wahl K, Crittenden RB, Bennett ML, *et al*: Astrocytic trans-differentiation completes a multicellular paracrine feedback loop required for medulloblastoma tumor growth. Cell 180: 502-520.e19, 2020.
19. Gandevia B and Tovell A: Declaration of Helsinki. Med J Aust 2: 320-321, 1964.
20. Eisen MB, Spellman PT, Brown PO and Botstein D: Cluster analysis and display of genome-wide expression patterns. Proc Natl Acad Sci USA 95: 14863-14868, 1998.
21. Pham CD, Flores C, Yang C, Pinheiro EM, Yearley JH, Sayour EJ, Pei Y, Moore C, McLendon RE, Huang J, *et al*: Differential immune microenvironments and response to immune checkpoint blockade among molecular subtypes of murine medulloblastoma. Clin Cancer Res 22: 582-595, 2016.
22. Graeber MB, Scheithauer BW and Kreutzberg GW: Microglia in brain tumors. Glia 40: 252-259, 2002.
23. McGranahan T, Therkelsen KE, Ahmad S and Nagpal S: Current state of immunotherapy for treatment of glioblastoma. Curr Treat Options Oncol 20: 24, 2019.
24. Northcott PA, Robinson GW, Kratz CP, Mabbott DJ, Pomeroy SL, Clifford SC, Rutkowski S, Ellison DW, Malkin D, Taylor MD, *et al*: Medulloblastoma. Nat Rev Dis Primers 5: 11, 2019.
25. Pugh TJ, Weeraratne SD, Archer TC, Pomeranz Krummel DA, Auclair D, Bochicchio J, Carneiro MO, Carter SL, Cibulskis K, Erlich RL, *et al*: Medulloblastoma exome sequencing uncovers subtype-specific somatic mutations. Nature 488: 106-110, 2012.
26. Nabors LB, Portnow J, Ammirati M, Baehring J, Brem H, Brown P, Butowski N, Chamberlain MC, Fenstermaker RA, Friedman A, *et al*: Central Nervous System Cancers, Version 1.2015. J Natl Compr Canc Netw 13: 1191-1202, 2015.
27. Palmer SL, Reddick WE and Gajjar A: Understanding the cognitive impact on children who are treated for medulloblastoma. J Pediatr Psychol 32: 1040-1049, 2007.
28. Lim M, Xia Y, Bettegowda C and Weller M: Current state of immunotherapy for glioblastoma. Nat Rev Clin Oncol 15: 422-442, 2018.
29. Becht E, Giraldo NA, Lacroix L, Buttard B, Elarouci N, Petitprez F, Selves J, Laurent-Puig P, Sautès-Fridman C, Fridman WH, *et al*: Estimating the population abundance of tissue-infiltrating immune and stromal cell populations using gene expression. Genome Biol 17: 218, 2016.
30. Liberzon A, Birger C, Thorvaldsdóttir H, Ghandi M, Mesirov JP and Tamayo P: The Molecular Signatures Database (MSigDB) hallmark gene set collection. Cell Syst 1: 417-425, 2015.
31. Lin GL, Nagaraja S, Filbin MG, Suvà ML, Vogel H and Monje M: Non-inflammatory tumor microenvironment of diffuse intrinsic pontine glioma. Acta Neuropathol Commun 6: 51, 2018.
32. Murata D, Mineharu Y, Arakawa Y, Liu B, Tanji M, Yamaguchi M, Fujimoto KI, Fukui N, Terada Y, Yokogawa R, *et al*: High programmed cell death 1 ligand-1 expression: Association with $CD8^+$ T-cell infiltration and poor prognosis in human medulloblastoma. J Neurosurg 128: 710-716, 2018.
33. Majzner RG, Simon JS, Grosso JF, Martinez D, Pawel BR, Santi M, Merchant MS, Geoerger B, Hezam I, Marty V, *et al*: Assessment of programmed death-ligand 1 expression and tumor-associated immune cells in pediatric cancer tissues. Cancer 123: 3807-3815, 2017.

34. Liang J, Piao Y, Holmes L, Fuller GN, Henry V, Tiao N and de Groot JF: Neutrophils promote the malignant glioma phenotype through S100A4. Clin Cancer Res 20: 187-198, 2014.
35. Quail DF and Joyce JA: The microenvironmental landscape of brain tumors. Cancer Cell 31: 326-341, 2017.
36. Margol AS, Robison NJ, Gnanachandran J, Hung LT, Kennedy RJ, Vali M, Dhall G, Finlay JL, Erdreich-Epstein A, Krieger MD, *et al*: Tumor-associated macrophages in SHH subgroup of medulloblastomas. Clin Cancer Res 21: 1457-1465, 2015.
37. Maximov V, Chen Z, Wei Y, Robinson MH, Herting CJ, Shanmugam NS, Rudneva VA, Goldsmith KC, MacDonald TJ, Northcott PA, *et al*: Tumour-associated macrophages exhibit anti-tumoural properties in Sonic Hedgehog medulloblastoma. Nat Commun 10: 2410, 2019.
38. Powell AB, Yadavilli S, Saunders D, Van Pelt S, Chorvinsky E, Burga RA, Albihani S, Hanley PJ, Xu Z, Pei Y, *et al*: Medulloblastoma rendered susceptible to NK-cell attack by TGFβ neutralization. J Transl Med 17: 321, 2019.
39. Nellan A, Rota C, Majzner R, Lester-McCully CM, Griesinger AM, Mulcahy Levy JM, Foreman NK, Warren KE and Lee DW: Durable regression of medulloblastoma after regional and intravenous delivery of anti-HER2 chimeric antigen receptor T cells. J Immunother Cancer 6: 30, 2018.